HFSS^{TM} Modelling Anomalies with THz Metal-Pipe Rectangular Waveguide Structures at Room Temperature

Yun Zhou and Stepan Lucyszyn
Imperial College London, UK

Abstract— Air-filled metal-pipe rectangular waveguides (MPRWGs) represent one of the most important forms of guided-wave structure for terahertz applications. Well-known commercial electromagnetic modelling software packages currently employ over-simplified intrinsic frequency dispersion models for the bulk conductivity of normal metals used in terahertz structures at room temperature. This paper has compared various conductivity modelling strategies for normal metals at room temperature and characterized rectangular waveguides and associated cavity resonators between 0.9 and 12 THz. An expression for the geometrical factor of a rectangular cavity resonator has been derived for the general case of a metal characterized with $\mu_r \neq 1$ and $\omega\tau > 0$. In addition, a method for determining the corresponding lossless frequency of oscillation had been given for the first time for such models. Using these techniques, a quantitative analysis for the application of different models used to describe the intrinsic frequency dispersion nature of bulk conductivity at room temperature has been undertaken. When compared to the use of the accurate relaxation-effect model, it has been found that HFSS^{TM} (Versions 10 and 11) gives a default error in the attenuation constant for MPRWGs of 108% at 12 THz and 41% errors in both Q-factor and overall frequency detuning with a 7.3 THz cavity resonator. With the former, measured transmission losses will be significantly lower than those predicted using the current version of HFSS^{TM}, which may lead to an underestimate of THz losses attributed to extrinsic effects. With the latter error, in overall frequency detuning, the measured positions of return loss zeros, within a multi-pole filter, will not be accurately predicted by the current version of HFSS^{TM}. This paper has highlighted a significant source of errors with the electromagnetic modeling of terahertz structures, operating at room temperatures, which can be rectified by adopting the classical relaxation-effect model to describe the frequency dispersive behavior of normal metals.

1. INTRODUCTION

The past decade has seen rapid developments in the exploitation of the lower terahertz frequency band [1–5]. Applications include radiometric imaging and remote sensing; spectroscopy and radio astronomy; as well as high-speed communications. Air-filled metal-pipe rectangular waveguides (MPRWGs) represent one of the most important forms of guided-wave structure for applications at (sub-)millimetre-wave frequencies. With the development of low-cost microfabrication technologies, high tolerance structures are becoming more affordable [6, 7]. This is helping to open up the lower terahertz frequency band to new, and possibly ubiquitous, applications in the not too distant future.

In addition to the advances being made for the manufacture of terahertz MPRWG structures [1–5], AB MILLIMETRE claim that their 8 GHz to 1 THz vector network analyzer (MVNA-8-350) can be pushed to perform measurements up to *ca.* 2 THz [8]. However, some well-known commercial electromagnetic modelling software packages currently employ over-simplified frequency dispersion models for the conductivity of metals used to predict the performance of terahertz structures at room temperature. For example, Ansoft's High Frequency Structure Simulator (HFSS^{TM}) is considered by some to represent a benchmark standard in electromagnetic modelling software, even though it can give anomalous results under certain conditions (e.g., electrically thin-walled MPRWGs [9]).

We investigate modelling anomalies found with HFSS^{TM} for the simulation of terahertz air-filled MPRWGs and associated cavity resonators. To this end, recommended standards for MPRWGs have been adopted here for operation between 0.9 and 12 THz, based on ISO 497:1973 *Preferred Metric Sizes* [10].

2. FREQUENCY DIPSERISON IN NORMAL METALS AT ROOM TEMPERATURE

For any normal metal at room temperature, the generic equations for intrinsic surface impedance Zs, propagation constant γ_s, skin depth δ_s and complex skin depth δ_c are given by:

$$
\begin{aligned}
&Z_S \equiv R_S + jX_S = \sqrt{\frac{j\omega\mu_0\mu_r}{\sigma + j\omega\varepsilon_o}} \cong \sqrt{\frac{j\omega\mu_0\mu_r}{\sigma}} \quad \text{with} \quad \omega < 10^{15}\ \text{rad/s} \\
&\gamma_S \equiv \alpha_S + j\beta_S = \frac{j\omega\mu_0\mu_r}{Z_S} = \sqrt{j\omega\mu_o\mu_r\sigma} \quad \text{and} \quad \delta_S = \frac{1}{\Re\{\gamma_S\}} = \frac{1}{\alpha_S} \quad \text{and} \quad \delta_c \equiv \delta_c' - j\delta_c'' = \frac{1}{\gamma_S}
\end{aligned} \tag{1}
$$

where $R_s = \Re\{Z_s\}$ is the surface resistance; $X_s = \Im\{Z_s\}$ is the surface reactance; $j = \sqrt{-1}$ is the complex operator; $\omega = 2\pi f$ is the angular frequency; f is the frequency of the driving electromagnetic field; μ_o is the permeability of free space; and μ_r is the relative permeability; σ is the intrinsic bulk conductivity of the metal; ε_o = permittivity of free space; $\alpha_S = \Re\{\gamma_S\}$ is the attenuation constant; and $\beta_S = \Im\{\gamma_S\}$ is the phase constant.

2.1. Intrinsic Frequency Dispersion Models for Normal Metals at Room Temperature

The "classical relaxation-effect model" (variables identified by the suffix R) is well understood and recognized as an analytical model that accurately describes the frequency dispersive nature of normal metals at room temperature [11, 12]. With the classical relaxation-effect (or Drude) model, intrinsic bulk conductivity is given by:

$$
\sigma_R \equiv \sigma_R' - j\sigma_R'' = \frac{\sigma_o}{(1 + j\omega\tau)} \Rightarrow \begin{cases} \sigma_R' = \frac{\sigma_o}{1+(\omega\tau)^2} & \text{Simple Relaxation-Effect Model} \\ \sigma_o & \text{Classical Skin-Effect Model} \end{cases} \tag{2}
$$

where, σ_o is the intrinsic bulk conductivity at DC; and τ is the phenomenological scattering relaxation time for the free electrons (i.e., mean time between collisions).

The "simple relaxation-effect model" (variables identified by the suffix R') takes only the real part of the conductivity from the classical relaxation-effect model. This model tried to remove the need for a complex conductivity, while still acknowledging that it has both a frequency and temperature dependency.

The "classical skin-effect model" (variables identified by the suffix o) removes the frequency dependency, while still keeping a temperature dependency. This model is traditionally used by RF, microwave and even millimeter-wave engineers, by default. With both the simple relaxation-effect and classical skin-effect models, equations for surface impedance, propagation constant and skin depth are greatly simplified; albeit overly-simplified at terahertz frequencies. Commercial electromagnetic modelling packages, such as HFSS$^{\text{TM}}$ (Versions 10 and 11), assume the classical skin-effect model by default, while giving the option to input frequency-dependent real values only for conductivity [13]. It should be noted here that HFSS$^{\text{TM}}$ (Versions 10 and 11) allows complex values for conductivity to be entered, but the imaginary term does not appear to be used in calculations.

The "effective relaxation-effect model" represents a logical way around the problem of not being able to incorporate the imaginary part of conductivity. It can be shown that the effective intrinsic bulk permittivity of the metal can be represented as:

$$
\varepsilon_{\mathit{eff}} = \varepsilon_o\varepsilon_{\mathit{reff}} \equiv \varepsilon_o(\varepsilon_{\mathit{reff}}' - j\varepsilon_{\mathit{reff}}'') = \sigma_{\mathit{eff}}/j\omega = \left[\sigma' + j(\omega\varepsilon_o - \sigma'')\right]/j\omega \tag{3}
$$

where $\varepsilon_{\mathit{reff}}$ is the effective relative intrinsic bulk permittivity of the metal (also know as the dielectric function), and the effective dielectric constant of the metal $\varepsilon_{\mathit{reff}}' = \Re\{\varepsilon_{\mathit{reff}}\}$ is given by:

$$
\varepsilon_{\mathit{reff}}' = 1 - \sigma''/\omega\varepsilon_o \tag{4}
$$

Therefore, with the effective relaxation-effect model, only the real values of intrinsic bulk conductivity and effective relative permittivity are needed to represent the classical relaxation-effect model. Unfortunately, it will be shown that with HFSS$^{\text{TM}}$ (Versions 10 and 11) this solution does not appear to work either, as the real part of effective relative intrinsic bulk permittivity also appears to be ignored for normal metals.

2.2. Surface Impedance and Skin Depth Calculations

Using (1)–(2), the surface impedance and skin depth can be easily defined and calculated for a normal metal at room temperature:

Classical relaxation-effect model: $\sigma(\omega) \rightarrow \sigma_R(\omega)$

$$\begin{aligned} Z_{SR} &\equiv R_{SR} + jX_{SR} = \sqrt{\frac{j\omega\mu_0\mu_r}{\sigma_R}} = Z_{So}\sqrt{1+ju}; \\ \delta_{SR} &= \frac{1}{\alpha_{SR}} = \Re\left\{\frac{j\omega\mu_o\mu_r}{Z_{SR}}\right\}^{-1} = \delta_{So}\sqrt{1+u^2}\frac{R_{SR}}{R_{So}} \quad \text{where} \quad u = (\omega\tau) \\ \delta_{cR} &= \frac{1}{\gamma_{SR}} = \sqrt{\frac{1+ju}{j\omega\mu_o\mu_r\sigma_o}} = \delta_{So}\frac{\sqrt{1+ju}}{(1+j)} = \frac{\delta_{So}}{j2}\sqrt{1+ju}\,(1+j) \\ &= \frac{\delta_{So}}{2}\left(\sqrt{\sqrt{1+u^2}+u} - j\sqrt{\sqrt{1+u^2}-u}\right) \end{aligned} \tag{5}$$

where $R_{SR} = R_{So}\sqrt{\sqrt{1+(\omega\tau)^2}-\omega\tau}$ is the surface resistance and $X_{SR} = R_{So}\sqrt{\sqrt{1+(\omega\tau)^2}+\omega\tau}$ is the surface reactance.

Simple relaxation-effect model: $\sigma(\omega) \rightarrow \sigma_{R'}(\omega)$

$$\begin{aligned} Z_{SR'} &\equiv R_{SR'} + jX_{SR'} = \sqrt{\frac{j\omega\mu_o\mu_r}{\sigma'_R}} = Z_{So}\sqrt{1+u^2}; \\ \delta_{SR'} &= \frac{1}{\alpha_{SR'}} = \frac{1}{\sigma'_R R_{SR'}} = \sqrt{\frac{2}{\omega\mu_o\mu_r\sigma'_R}} = \delta_{So}\sqrt{1+u^2} \\ \delta_{cR'} &= \frac{1}{\gamma_{SR'}} = \sqrt{\frac{1+u^2}{j\omega\mu_o\mu_r\sigma_o}} = \delta_{So}\frac{\sqrt{1+u^2}}{(1+j)} = \frac{\delta_{So}}{2}\sqrt{1+u^2}(1-j) = \frac{\delta_{SR'}}{2}(1-j) \end{aligned} \tag{6}$$

where $R_{SR'} = R_{So}\sqrt{1+(\omega\tau)^2}$ is the surface resistance and $X_{SR'} \equiv R_{SR'}$ is the surface reactance.

Classical skin-effect model: $\sigma(\omega) \rightarrow \sigma_o$

$$\begin{aligned} Z_{So} &\equiv R_{So} + jX_{So} = \sqrt{\frac{j\omega\mu_o\mu_r}{\sigma_o}} = R_{So}\,(1+j)\,; \\ \delta_{So} &= \frac{1}{\alpha_{So}} = \frac{1}{\sigma_o R_{So}} = \sqrt{\frac{2}{\omega\mu_o\mu_r\sigma_o}} \\ \delta_{co} &= \frac{1}{\gamma_{So}} = \sqrt{\frac{1}{j\omega\mu_o\mu_r\sigma_o}} = \frac{\delta_{So}}{(1+j)} = \frac{\delta_{So}}{2}(1-j) \end{aligned} \tag{7}$$

where $R_{So} = \sqrt{\frac{\omega\mu_o\mu_r}{2\sigma_o}}$ is the surface resistance and $X_{So} \equiv R_{So}$ is the surface reactance.

For gold at room temperature, the electrical parameters may differ between published sources; depend on the exact temperature and method of deposition [11, 13, 14]. The values adopted here for bulk DC conductivity, relative permeability and relaxation time are $\sigma_o = 4.517 \times 10^7\,\mathrm{S/m}$, $\mu_r = 0.99996$ and $\tau = 27.135fs$, respectively. In order to be consistent, these values have been used in all methods of modelling (i.e., in both calculations and HFSS$^{\mathrm{TM}}$ simulations). Fig. 1 shows the calculated values from 0.9 to 12 THz for gold at room temperature for surface resistance, surface reactance, skin depth and the imaginary part of complex skin depth.

It can be seen from Fig. 1(a) that all three models give diverging values for surface resistance as frequency increases. Indeed, contrary to normal expectations, the rise in value for the relaxation-effect model is much less than with the other models; resulting in lower levels of predicted attenuation and higher unloaded Q-factors with the relaxation-effect model for MPRWG structures. From Fig. 1(b), it can be seen that surface reactance is very similar for both classical and simple relaxation-effect models, and these have a much greater increase with frequency when compared to the classical skin-effect model; resulting in higher levels of predicted frequency detuning error with the classical skin-effect model for cavity resonators.

With reference to Fig. 1(c), both classical relaxation- and skin-effect models give similar reductions in skin depth $\delta_S(\omega)$ with frequency. However, with the simple relaxation-effect model, there is a turning point at the relaxation frequency $f_\tau = 5.865\,\mathrm{THz}$; above which the skin depth begins

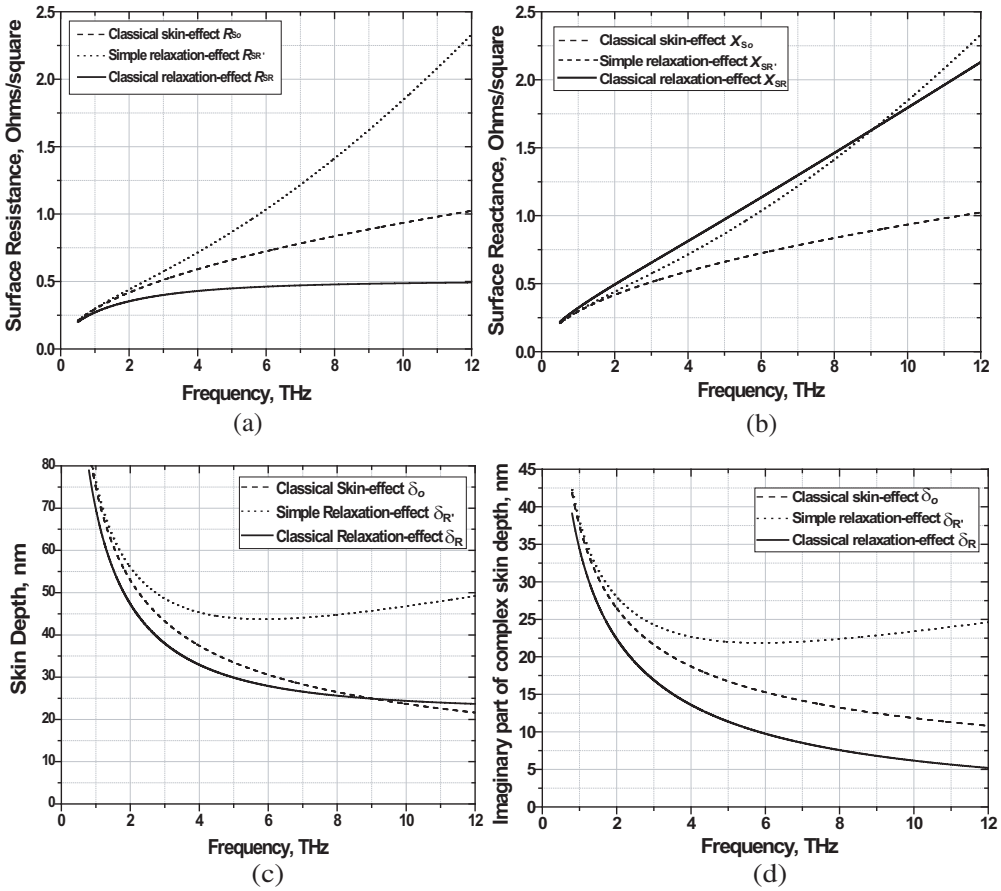

Figure 1: Calculated values for gold at room temperature: (a) surface resistance; (b) surface reactance; (c) skin depth; and (d) imaginary part of complex skin depth.

to increase with frequency — contrary to conventional expectations. It will be seen in Section 4 that, for the general case of a metal with $\omega\tau > 0$, the unloaded Q-factor is inversely proportional to the imaginary part of the complex skin depth $\Im\{\delta_c(\omega)\}$; this has been plotted in Fig. 1(d). It can be seen that while the simple relaxation- and classical skin-effect models have frequency responses that scale those of skin depth, the classical relaxation-effect model has its imaginary part of complex skin depth that decreases much more than with the other models. This will result in higher levels of unloaded Q-factor and significant errors with the simple relaxation- and classical skin-effect models for cavity resonators.

3. THZ METAL-PIPE RECTANGULAR WAVEGUIDE MODELLING

3.1. Proposed ISO 497:1973-based Standards for THz Frequencies

In Fig. 2, a uniform air-filled MPRWG is defined within the Cartesian coordinate system xyz. Transmission is along the z direction, and over a distance d, with internal cross-sectional dimensions a and b.

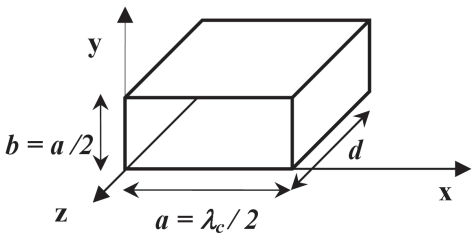

Figure 2: Internal spatial variable definitions for a uniform air-filled MPRWG.

The structure in Fig. 2 has the ideal (i.e., lossless) dominant-mode guided wavelength given by the following textbook expression [15]:

$$\lambda_{g\_ideal} = \frac{\lambda_o}{\sqrt{1-\left(\frac{\lambda_o}{\lambda_c}\right)^2}} = \frac{\lambda_o}{\sqrt{1-\left(\frac{f_c}{f}\right)^2}} \tag{8}$$

where, λ_o is the free space wavelength; $\lambda_c = 2a$ is the ideal cut-off wavelength; a is the internal width dimension of the MPRWG; $f_c = c/2a$ is the ideal cut-off frequency for the dominant TE_{10} mode; and c is the speed of light in free space.

For many decades, MPRWGs have been standardized by different designations (e.g., IEC-R, EIA-WR and WG). Currently, commercialization of such waveguides exists up to 500 GHz (i.e., WR-2.2) by Millitech® [15] and up to 1.157 THz (i.e., WR-0.51) by Virginia Diodes Inc. [16]. However, there are still no global standards for frequency bands at terahertz frequencies. Cross-sectional dimension variations between well-established standards create serious problems, which are exacerbated by inadequate mechanical tolerances, as frequencies approach the terahertz spectrum. In order to provide compatible (interchangeable) hardware at terahertz frequencies, the width dimension can be generated using the ISO 497:1973 *Preferred Metric Sizes* standard [10]; as recently proposed for operational frequencies between 0.9 and 2.9 THz [17, 18]. The ISO 497:1973 standard is already adopted widely by industry for other applications, is infinitely extendable and finer choices can accommodate smaller dimensions. Based on this standard, as shown in Table 1, we have extended the four lower terahertz frequency bands [17, 18] up to 12 THz.

Table 1: Proposed air-filled MPRWG and cavity resonator definitions and specifications.

ISO 497 Preferred Metric Size		Proposed Frequency Band Designation (μm)		Internal Dimensions $a \times b$ (μm²)	TE_{10} -mode Ideal Cutoff Frequency f_C (THz)	Lower-Band Frequency Factor f_L / f_C	Mid-Band Frequency $f_O = 1.55 f_C$ (THz)	Upper-Band Frequency Factor f_U / f_C	Useful Frequency Range $f_L \rightarrow f_U$ (THz)	TE_{101}-mode Ideal Cavity Resonance Frequency $f_{101\_ideal} = \sqrt{1.5} f_c$ (THz)
B	*i*	JPL	Our							
20'	6	200		200×100	0.75	1.20	1.162	1.93	0.90→1.45	0.919
20'	4	160		160×80	0.94	1.23	1.452	1.92	1.15→1.80	1.148
20'	2	125		125×62.5	1.20	1.21	1.860	1.92	1.45→2.30	1.470
20'	0	100		100×50	1.50	1.20	2.325	1.93	1.80→2.90	1.837
40	35		75	75×32.5	2.00	1.20	3.100	1.90	2.40→4.00	2.449
20'	14		50	50×25	3.00	1.20	4.650	1.90	3.60→6.00	3.674
20'	10		32	32×16	4.68	1.20	7.260	1.90	5.62→8.90	5.732
20'	8		25	25×12.5	6.00	1.20	9.300	1.90	7.20→12.00	7.348

3.2. Calculation of Attenuation Constant

The propagation constant for a lossy metal-pipe rectangular waveguide can be accurately calculated using the *variational* method [19] for the TE_{mo} mode [7], as follows:

$$\begin{aligned} \gamma_{mo}^2 &= \Gamma_d^2 - j\frac{2Z_s}{\omega\mu_o\mu_r b}\left[\left(\frac{\Gamma_d}{k_c}\frac{m\pi}{a}\right)^2 - k_c^2\left(1+\frac{2b}{a}\right)\right]; \quad \Gamma_d^2 = k_c^2 - k_{od}^2 \\ k_c &= \omega_c\sqrt{\mu_o\mu_r\varepsilon_o\varepsilon_r} \rightarrow \omega_c\sqrt{\mu_o\varepsilon_o} = \frac{\omega_c}{c} \quad \text{in free space} \\ k_{od} &= \omega\sqrt{\mu_o\mu_r\varepsilon_o\varepsilon_r\left(1-j\tan\delta\right)} \rightarrow k_o = \omega\sqrt{\mu_o\varepsilon_o} = \frac{\omega}{c} \quad \text{in free space} \end{aligned} \tag{9}$$

where ε_r is the dielectric constant and $\tan\delta$ is the loss tangent for the dielectric filler.

The attenuation constant for this guided-wave structure can be obtained directly from the real part of the propagation constant, i.e., $\alpha = \Re\{\gamma_{mo}\}$. For the dominant TE_{10} mode, the following expressions for attenuation constant can be calculated, based on the intrinsic frequency dispersion models for normal metals at room temperature.

Classical relaxation-effect model

$$\alpha_R = \Re\{\gamma_{10R}\}; \quad \gamma_{10R} = f\{Z_{SR}\} \tag{10a}$$

Simple relaxation-effect model

$$\alpha_{R'} = \Re\{\gamma_{10R'}\}; \quad \gamma_{10R'} = f\{Z_{SR'}\} \tag{10b}$$

Classical skin-effect model

$$\alpha_o = \Re\{\gamma_{10o}\}; \quad \gamma_{10o} = f\{Z_{So}\} \tag{10c}$$

Using (10) with the simple Power Loss approximation method, as used in [6], for calculating attenuation constant in terms of the real part of the surface impedance only, it is easy to calculate the percentage error in attenuation constant for the simple relaxation-effect model $E_{\alpha_{R'}}$ and classical skin-effect model E_{α_o}, relative to the classical relaxation-effect model, as follows:

$$\begin{aligned} E_{\alpha_{R'}} &= \left(\frac{\alpha_{R'} - \alpha_R}{\alpha_R}\right) \cdot 100\% \cong \left[\sqrt{\frac{1+(\omega\tau)^2}{\sqrt{1+(\omega\tau)^2}-\omega\tau}} - 1\right] \cdot 100\% \\ E_{\alpha_o} &= \left(\frac{\alpha_o - \alpha_R}{\alpha_R}\right) \cdot 100\% \cong \left[\sqrt{\sqrt{1+(\omega\tau)^2}+\omega\tau} - 1\right] \cdot 100\% \end{aligned} \tag{11}$$

For simplicity, it will be assumed throughout that the MPRWGs will have a height dimension of $b = a/2$. The attenuation constants and resulting errors have been plotted against frequency, and are shown in Fig. 3. To a first degree of approximation, it can be seen that the error increases linearly with frequency for the classical skin-effect model; with a 108% error at 12 THz. The error obtained with the simple relaxation-effect model is 373% at 12 THz.

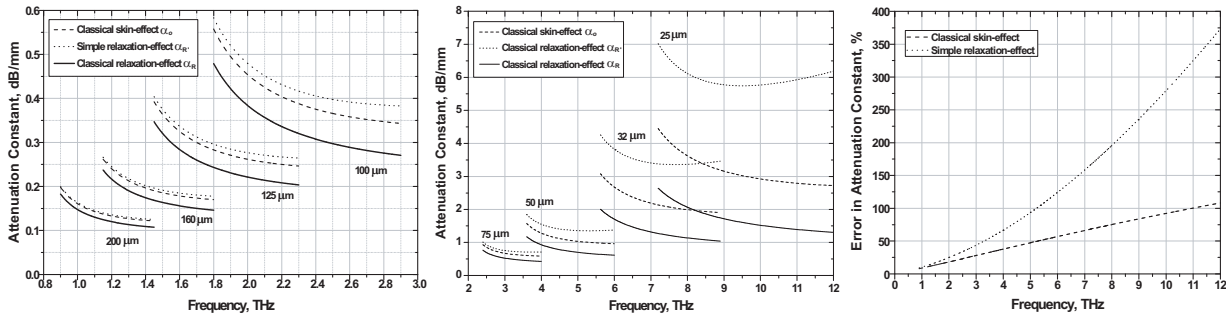

Figure 3: Calculated attenuation constants for the dominant TE_{10} mode: (a) JPL bands; (b) our bands; and (c) resulting errors in attenuation constants.

3.3. Electromagnetic Simulation of Attenuation Constant

$HFSS^{TM}$ is often used to design terahertz guided-wave structures [1–5]. Therefore, to test its suitability at these frequencies, a number of simple, uniform THz air-filled MPRWGs were simulated. The $HFSS^{TM}$ results are shown in Fig. 4(a), while the calculated values are superimposed, for comparison, in Fig. 4(b). It can be clearly seen in Fig. 4 that all the relaxation-effect model values entered into $HFSS^{TM}$ give identical results to the calculated simple relaxation-effect model, while $HFSS^{TM}$ (by default) gives results that conform to the calculated classical skin-effect model. This clearly shows that $HFSS^{TM}$ (Versions 10 and 11) cannot give accurate results and that very large errors will result, corresponding to those given in Fig. 3(c).

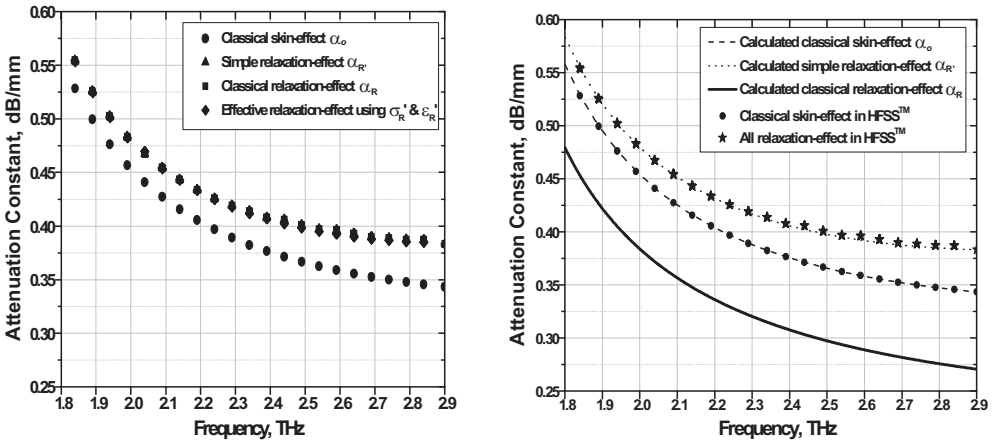

(a) (b)

Figure 4: HFSS$^{\text{TM}}$ simulated attenuation constant for the dominant TE_{10} mode in the JPL bands: (a) HFSS$^{\text{TM}}$ only; and (b) HFSS$^{\text{TM}}$ and calculated values.

4. THZ CAVITY RESONATOR MODELLING

4.1. Derivation of Basic Equations

With reference to Fig. 2, the internal dimensions of a cavity resonator are a, b and d. The corresponding textbook expression for the resonant frequencies for the TE_{mnl} modes in an ideal (i.e., lossless) cavity is give by:

$$f_{mnl\_ideal} = \frac{c}{2\pi}\sqrt{\left(\frac{m\pi}{a}\right)^2 + \left(\frac{n\pi}{b}\right)^2 + \left(\frac{l\pi}{d}\right)^2} \tag{12}$$

For simplicity, it will be assumed throughout that the cavity will have spatial dimensions of $b = a/2$ and $d = \sqrt{2}a$. Moreover, only the dominant TE_{101} mode will be considered:

$$\therefore f_{101\_ideal} = \sqrt{1.5} f_c = \sqrt{\frac{3}{8}}\left(\frac{c}{a}\right) \equiv \frac{\omega_I}{2\pi} \tag{13}$$

In HFSS$^{\text{TM}}$, the eigenmode solver determines the complex resonant frequency of a structure $\tilde{\omega}_o$ [20]:

$$\begin{aligned} \tilde{\omega}_o &\equiv \omega_o' + j\omega_o'' = \omega_o\sqrt{1 - \left(\frac{1}{2Q_u(\omega_o)}\right)^2} + j\frac{\omega_o}{Q_u(\omega_o)} \\ \omega_o &= |\tilde{\omega}_o| = \sqrt{(\omega_o')^2 + (\omega_o'')^2} \quad \text{and} \quad Q_u(\omega_o) = \frac{\omega_o}{2\omega_o''} \end{aligned} \tag{14}$$

With a non-zero surface reactance, the equivalent surface inductance effectively reduces the lossless frequency of oscillation ω_o from the ideal case ω_I by a small perturbation, $\Delta\omega_I = (\omega_o - \omega_I)$. Moreover, with most applications, the unloaded Q-factor $Q_u(\omega_o)$ is large enough so that the corresponding frequency detuning caused by ohmic losses (e.g., surface resistance) is negligible, such that $\omega_o' \cong \omega_o$. It has been shown by Slater [20] that, to the first order of small quantities:

$$\tilde{\omega}_o = \omega_o + j\frac{\omega_I}{2Q_u(\omega_o)} \quad \text{where} \quad \omega_I = \pi\sqrt{\frac{3}{2}}\left(\frac{c}{a}\right) \tag{15}$$

$$\text{when} \quad \sigma_o \to \infty: \quad \omega_o \to \omega_I \quad \text{and} \quad Q_U(\omega_I) \to \infty: \quad \Delta\tilde{\omega}_o = (\omega_o - \omega_I) + j\frac{\omega_I}{2Q_u(\omega_o)} \tag{16}$$

Now, the cavity perturbation formula can be used to relate the change in complex resonant frequency to the corresponding change in surface impedance, as follows [20]:

$$\Delta Z_S = -j2\Gamma \cdot \Delta\tilde{\omega}_o \tag{17}$$

It can be shown that, for the general case, the geometrical factor Γ is given by:

$$\Gamma = \mu_0 \left\{ \frac{abd\left(a^2+d^2\right)}{2\left[2b\left(a^3+d^3\right)+ad\left(a^2+d^2\right)\right]} \right\} = \mu_0 \left(\frac{3a}{2(\sqrt{2}+10)} \right) \tag{18}$$

But, when $\sigma_o \to \infty$: $\quad Z_S(\omega_I) \to 0 \quad \Delta Z_S = Z_S(\omega_o)$:

$$\begin{aligned} \therefore Z_S\left(\omega_o\right) &= \omega_I \Gamma \left(\frac{1}{Q_u\left(\omega_o\right)} + j \frac{2\left(\omega_I - \omega_o\right)}{\omega_I} \right) \\ \text{where} \qquad R_S\left(\omega_o\right) &= \frac{\omega_I \Gamma}{Q_u\left(\omega_o\right)} \quad \text{and} \quad X_S\left(\omega_o\right) = 2\Gamma\left(\omega_I - \omega_o\right) \end{aligned} \tag{19}$$

We have found that for the general case of a metal with $\mu_r \neq 1$ and $\omega\tau > 0$, in order to achieve a self-consistent solution, the unloaded Q-factor can be expressed as follows:

$$\begin{aligned} Q_u\left(\omega_o\right) &= \frac{\lambda_I(\omega_I)}{8\mu_r \Im\left\{\delta_c\left(\omega_o\right)\right\}} \left(\frac{\omega_I}{\omega_o}\right) \left\{ \frac{2b\left(a^2+d^2\right)^{\frac{3}{2}}}{\left[2b\left(a^3+d^3\right)+ad\left(a^2+d^2\right)\right]} \right\} \\ &= \frac{1}{\mu_r \Im\left\{\delta_c(\omega_o)\right\}} \left(\frac{\omega_I}{\omega_o}\right) \left(\frac{3\sqrt{2}a}{4\left(5\sqrt{2}+1\right)} \right) \\ \text{where} \qquad \delta_c(\omega_o) &\equiv \delta_c'(\omega_o) - j\delta_c''(\omega_o) = \frac{1}{\gamma_S(\omega_o)} \end{aligned} \tag{20}$$

Now, the frequency of oscillation ω_o' is defined in (14). The overall frequency detuning, which takes both perturbation and frequency detuning due to ohmic losses into account, is given by $\Delta\omega_o' = (\omega_o' - \omega_I)$. The corresponding errors in overall frequency detuning, relative to the classical relaxation-effect model, are given by:

$$\begin{aligned} E_\omega &= \left| \frac{\Delta\omega_o' - \Delta\omega_{oR}'}{\Delta\omega_{oR}'} \right| \times 100\% = \left| \frac{\omega_o' - \omega_{oR}'}{\omega_{oR}' - \omega_I} \right| \times 100\% \\ \text{where} \qquad \Delta\omega_{oR}' &= \left(\omega_{oR}' - \omega_I\right) \quad \text{and} \quad \Delta\omega_o' \to \Delta\omega_{oo}' = \left(\omega_{oo}' - \omega_I\right) \quad \text{or} \quad \Delta\omega_{oR'}' = \left(\omega_{oR'}' - \omega_I\right) \end{aligned} \tag{21}$$

At the frequency of oscillation:

$$\begin{aligned} \therefore Q_u\left(\omega_o'\right) &= \frac{\omega_I \Gamma}{R_S\left(\omega_o'\right)} = \frac{1}{\mu_r \Im\left\{\delta_c\left(\omega_o'\right)\right\}} \left(\frac{\omega_I}{\omega_o'}\right) \left(\frac{3\sqrt{2}a}{4\left(5\sqrt{2}+1\right)} \right) \\ \text{where} \qquad \delta_c(\omega_o') &\equiv \delta_c'(\omega_o') - j\delta_c''(\omega_o') = \frac{1}{\gamma_S(\omega_o')} \end{aligned} \tag{22}$$

The corresponding errors in unloaded Q-factor, relative to the classical relaxation-effect model, are given by:

$$\begin{aligned} E_Q &= \left| \frac{Q_U(\omega_o') - Q_{UR}(\omega_{oR}')}{Q_{UR}(\omega_{oR}')} \right| \times 100\% = \left| \left(\frac{R_{SR}(\omega_{oR}')}{R_S(\omega_o')} \right) - 1 \right| \times 100\% \\ \text{where} \qquad Q_U(\omega_o') &\to Q_{Uo}(\omega_{oo}') \quad \text{or} \quad Q_{UR'}(\omega_{oR'}') \quad \text{and} \quad R_S(\omega_o') \to R_{So}(\omega_{oo}') \quad \text{or} \quad R_{SR'}(\omega_{oR'}') \end{aligned} \tag{23}$$

4.2. Derivation of Lossless Frequency of Oscillation

In order to determine the level of unloaded Q-factor and overall frequency detuning, both at the frequency of oscillation, it is first necessary to determine the lossless frequency of oscillation and then the unloaded Q-factor at this frequency, so that the frequency of oscillation can be found using (14). To this end, by equalizing equations for surface reactance, the lossless frequency of oscillation can be found by solving the roots of the characteristic equation given for each of the intrinsic frequency dispersion model.

The classical relaxation-effect model: $\omega_o \to \omega_{oR}$

$$\begin{aligned} & X_{SR}(\omega_{oR}) = R_{So}(\omega_{oR}) \sqrt{\sqrt{1+(\omega_{oR}\tau)^2} + \omega_{oR}\tau} \equiv 2\Gamma\left(\omega_I - \omega_{oR}\right) \\ \therefore & \frac{\sqrt{\omega_{oR}\left(\sqrt{1+(\omega_{oR}\tau)^2} + \omega_{oR}\tau\right)}}{\left(\omega_I - \omega_{oR}\right)} - K \equiv 0 \quad \text{where} \quad K = \sqrt{\frac{8\mu_o\sigma_o}{\mu_r}} \cdot \left(\frac{3a}{2(\sqrt{2}+10)} \right) \end{aligned} \tag{24}$$

For the simple relaxation-effect model: $\omega_o \rightarrow \omega_{oR'}$

$$X_{SR'}(\omega_{oR'}) = R_{So}(\omega_{oR'})\sqrt{1+(\omega_{oR'}\tau)^2} \equiv 2\Gamma\left(\omega_I - \omega_{oR'}\right)$$
$$\therefore \cdot \frac{\sqrt{\omega_{oR'}\left(1+(\omega_{oR'}\tau)^2\right)}}{\left(\omega_I - \omega_{oR'}\right)} - K \equiv 0 \tag{25}$$

For the classical skin-effect model: $\omega_o \rightarrow \omega_{oo}$

$$X_{So}(\omega_{oo}) = \sqrt{\frac{\omega_{oo}\mu_o\mu_r}{2\sigma_o}} \equiv 2\Gamma\left(\omega_I - \omega_{oo}\right)$$
$$\therefore \frac{\sqrt{\omega_{oo}}}{\left(\omega_I - \omega_{oo}\right)} - K \equiv 0$$
$$\omega_{oo} = (W+\omega_I) - \sqrt{(W+\omega_I)^2 - \omega_I^2} \quad \text{where} \quad W = \frac{1}{2K^2} \tag{26}$$

4.3. Calculation and Electromagnetic Simulation of Unloaded Q-factor and Frequency Detuning

The calculated and HFSS^{TM} simulated values for unloaded Q-factor and overall frequency detuning are plotted in Fig. 5(a), for rectangular waveguide cavity resonators operating in the dominant TE_{101} mode. It can be seen that the results from HFSS^{TM} correspond exactly to those calculated using the classical skin-effect model. As previously explained in Section 2.2, the classical relaxation-effect model will predict higher unloaded Q-factor and overall frequency detuning, when compared to the other models.

The resulting errors in unloaded Q-factor and overall frequency detuning, relative to the classical relaxation-effect model, show an almost identical frequency response for both with the classical skin-effect model. Here, a 41% error is calculated for a 7.3 THz cavity resonator. This level of error in overall frequency detuning can have a dramatic impact on the positions of return loss zeros, within a multi-pole filter. A much lower error is found in the overall frequency detuning with the simple relaxation-effect model; with a worst-case value of 12% for a 3.7 THz cavity resonator. However, a 63% error in the unloaded Q-factor has been calculated with the simple relaxation-effect model for a 7.3 THz cavity resonator.

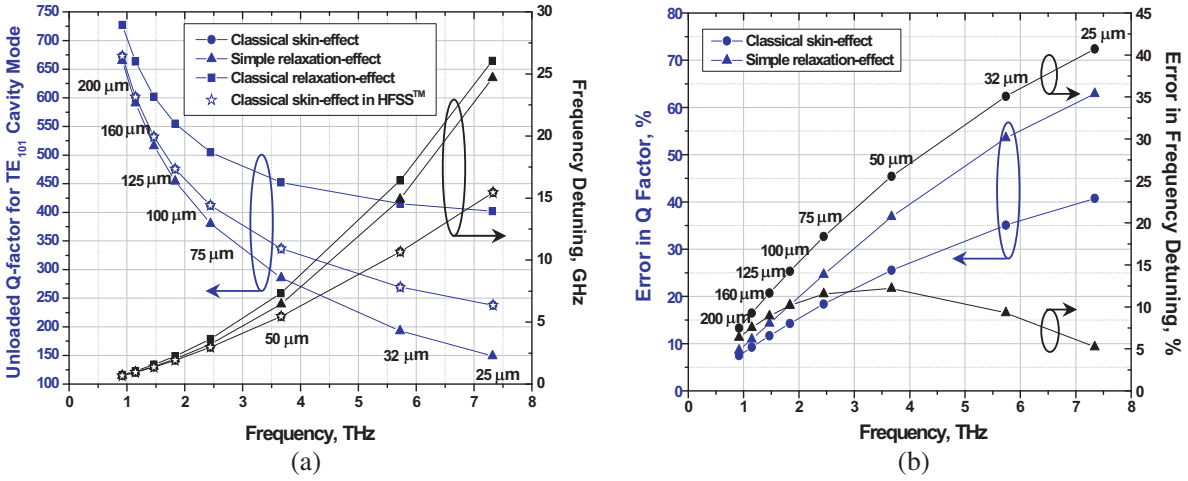

Figure 5: (a) Unloaded Q-factor and overall frequency detuning for TE_{101} cavity mode, at the resonant frequencies; and (b) resulting errors in Q factors and frequency detuning.

5. CONCLUSIONS

This paper has compared various conductivity modelling strategies for normal metals at room temperature and characterized rectangular waveguides and associated cavity resonators between 0.9 and 12 THz. It has been found that the current versions of HFSS^{TM} (Versions 10 and 11) cannot

accurately predict the performance of structures operating at terahertz frequencies. For example, with simple uniform MPRWGs, measured transmission losses can be significantly lower, which may lead to an underestimate of THz losses attributed to extrinsic effects; such as poor mechanical tolerances and surface roughness. Also, from the errors found in the frequency detuning of simple rectangular cavity resonators, the measured positions of return loss zeros, within a multi-pole filter, will not be accurately predicted.

It should be noted that while this paper has focused on the current version of HFSS^{TM}, the same problem can be found with other commercial electromagnetic modelling software packages that use the overly-simplified classical skin-effect model by default. This paper has highlighted a significant source of errors with the electromagnetic modeling of terahertz structures, operating at room temperatures, which can be rectified by adopting the classical relaxation-effect model to describe the frequency dispersive behavior of normal metals.

ACKNOWLEDGMENT

This work was supported by the UK's Engineering and Physical Sciences Research Council (EPSRC) under Platform Grant EP/E063500/1.

REFERENCES

1. Kazemi, H., S. T. Wootton, N. J. Cronin, S. R. Davies, R. E. Miles, R. D. Pollard, J. M. Chamberlain, D. P. Steenson and J. W. Bowen, "Active micromachined integrated terahertz circuits," *International Journal of Infrared and Millimeter Waves*, Vol. 20, No. 5, 967–974, Mar. 1999.
2. Maiwald, F., S. Martin, J. Bruston, A. Maestrini, T. Crawford and P. H. Siegel, "2.7 THz waveguide tripler using monolithic membrane diodes," *IEEE MTT-S International Microwave Symposium Digest*, Vol. 3, 1637–1640, May 2001.
3. Pavolotsky, A., D. Meledin, C. Risacher, M. Pantaleev, and V. Belitsky, "Micromachining approach in fabricating of THz waveguide components," *Microelectronics J.*, Vol. 36, 683–686, Jun. 2005.
4. Bowen, J. W., S. Hadjiloucas, B. M. Towlson, L. S. Karayzas, S. T. G. Wootton, N. J. Cronin, S. R. Davies, C. E. McIntosh, J. M. Chamberlain, R. E. Miles, and R. D. Pollard, "Micromachined waveguide antennas for 1.6 THz," *IET Electronics Letters*, Vol. 42, No. 15, 842–843, Jul. 2006.
5. Nordquist, C. D., M. C. Wanke, A. M. Rowen, C. L. Arrington, M. Lee, and A. D. Grine, "Design, fabrication, and characterization of metal micromachined rectangular waveguides at 3 THz," *Antennas and Propagation Society International Symposium (AP-S 2008)*, 1–4, Jul. 2008.
6. Lucyszyn, S., Q. H. Wang, and I. D. Robertson, "0.1 THz rectangular waveguide on GaAs semi-insulating substrate," *IEE Electronics Letters*, Vol. 31, No. 9, 721–722, Apr. 1995.
7. Lucyszyn, S., D. Budimir, Q. H. Wang, and I. D. Robertson, "Design of compact monolithic dielectric-filled metal-pipe rectangular waveguides for millimetre-wave applications," *IEE Proceedings — Microwaves, Antennas and Propagation*, Vol. 143, No. 5, 451–453, Oct. 1996.
8. http://www.abmillimetre.com/Products.htm.
9. Choi, J. Y. and S. Lucyszyn, "HFSS^{TM} modelling anomalies with electrically thin-walled metal-pipe rectangular waveguide simulations," *10th IEEE High Frequency Postgraduate Student Colloquium (10th HF-PgC) Digest*, 95–98, ISBN: 0-7803-9500-X, Leeds, Sep. 2005.
10. ISO 497:1973, "Guide to the choice of series of preferred numbers and of series containing more rounded values of preferred numbers," 1973. http://www.iso.org/iso/iso_catalogue/catalogue_tc/catalogue_detail.htm?csnumber=4548
11. Lucyszyn, S., "Investigation of anomalous room temperature conduction losses in normal metals at terahertz frequencies," *IEE Proceedings — Microwaves, Antennas and Propagation*, Vol. 151, No. 4, 321–329, Aug. 2004.
12. Lucyszyn, S., "Investigation of Wang's model for room temperature conduction losses in normal metals at terahertz frequencies," *IEEE Trans. on Microwave Theory Tech.*, Vol. 53, 1398–1403, Apr. 2005.
13. HFSS^{TM} help files for versions 10 & 11.
14. Lide, D. R. (Editor-in-chief), *CRC Handbook of Chemistry and Physics*, CRC Press, 2003.
15. Millitech® Inc., "Rectangular waveguide specifications and MIL-specification cross reference". http://www.millitech.com/pdfs/recspec.pdf

16. Virginia Diodes Inc., "Waveguide band designations". http://www.vadiodes.com/VDI/pdf/VDI%20Waveguide%20Chart.pdf
17. Ward, J. S., "New standards for submillimeter wavelengths," *17th International Symposium on Space Terahertz Technology*, Paris, May 2006.
18. Ward, J. S., "Terahertz waveguide standards," *IEEE MTT-S International Microwave Symposium Workshop*, WFD 06-2, San Francisco, USA, 2006.
19. Collin, R. E., *Field Theory of Guide Waves*, 182–195, McGraw-Hill, 1960.
20. Slater, J. C., "Microwave electronics," *Rev. of Modern Physics*, Vol. 18, No. 4, 441–512, Oct. 1946.